A Statistical Method for Generating Temporally Downscaled Geochemical Tracers in Precipitation

Catherine E. Finkenbiner[1], Stephen P. Good[1], Scott T. Allen[2], Richard P. Fiorella[3], Gabriel J. Bowen[3]

[1]*Department of Biological and Ecological Engineering, Oregon State University, Corvallis, OR*

[2]*Department of Natural Resources and Environmental Science, University of Nevada, Reno, NV*

[3]*Department of Geology and Geophysics, University of Utah, Salt Lake City, UT*

Corresponding Author: Catherine Finkenbiner, c.finkenbiner@gmail.com

Early Online Release: This preliminary version has been accepted for publication in *Journal of Hydrometeorology,* may be fully cited, and has been assigned DOI 10.1175/JHM-D-20-0142.1. The final typeset copyedited article will replace the EOR at the above DOI when it is published.

ABSTRACT

Sampling intervals of precipitation geochemistry measurements are often coarser than those required by fine-scale hydrometeorological models. This study presents a statistical method to temporally downscale geochemical tracer signals in precipitation so that they can be used in high-resolution, tracer-enabled applications. In this method, we separated the deterministic component of the time series and the remaining daily stochastic component, which was approximated by a conditional multivariate Gaussian distribution. Specifically, statistics of the stochastic component could be explained from coarser data using a newly identified power-law decay function, which relates data aggregation intervals to changes in tracer concentration variance and correlations with precipitation amounts. These statistics were used within a copula framework to generate synthetic tracer values from the deterministic and stochastic time series components based on daily precipitation amounts. The method was evaluated at 27 sites located worldwide using daily precipitation isotope ratios, which were aggregated in time to provide low resolution testing datasets with known daily values. At each site, the downscaling method was applied on weekly, biweekly and monthly aggregated series to yield an ensemble of daily tracer realizations. Daily tracer concentrations downscaled from a biweekly series had average (+/- standard deviation) absolute errors of 1.69‰ (1.61‰) for δ^2H and 0.23‰ (0.24‰) for δ^{18}O relative to observations. The results suggest coarsely sampled precipitation tracers can be accurately downscaled to daily values. This method may be extended to other geochemical tracers in order to generate downscaled datasets needed to drive complex, fine-scale models of hydrometeorological processes.

Accepted for publication in *Journal of Hydrometeorology*. DOI 10.1175/JHM-D-20-0142.1.

1. Introduction

Naturally occurring chemical signatures in precipitation (e.g. Bailey et al. 2018, Bowen et al. 2019, Gibson et al. 2005, Kendall and McDonnell 2012, Moerman et al. 2013, West et al. 2010, Wiederhold 2015) are frequently used as hydrometeorological tracers, especially when inferring transport or chemical transformations through terrestrial, aquatic, and atmospheric environments (e.g. Abbott et al. 2016, Brooks et al. 2014, Good et al. 2015, Gupta et al. 2020, Kanner et al. 2014, Remondi et al. 2018). Tracer-enabled modeling allows for process-level inference based not only on the size of fluxes, but also on the spatial and temporal transport and mixing of the geochemical signatures associated with the fluxes, thereby facilitating improved understanding and multi-response model evaluation (Bowen and Good 2015, Krause et al. 2005, McGuire and McDonnell 2006, Sprenger et al. 2019, Turnadge and Smerdon 2014). Researchers have used tracers within global climate models to evaluate processes that are challenging to observe (e.g. ageostrophic circulations, convection and turbulence) or are modeled at sub-grid scales and are therefore not explicitly simulated but parameterized (e.g. Gupta et al. 2020, Orbe et al. 2020, Rosa et al. 2012). For instance, isotope-enabled general circulation models (GCMs) have explicitly simulated water isotope ratios within the critical zone on sub-daily time scales (e.g., a version of the Community Earth System Model (iCESM1); Brady et al. 2019, Nusbaumer et al. 2017, Wong et al. 2017) and provide outputs which have been evaluated against observational datasets at various scales (e.g., Hoffmann et al. 2000, Nusbaumer et al. 2017, Risi et al. 2012, Steen-Larsen et al. 2016, Wong et al. 2017).

In many modeling applications, observed and modeled temporal resolutions are different and, in these cases, a downscaling method is required in order to use observed datasets within a model to evaluate processes with dynamic fluctuations over short temporal intervals (Ebtehaj and

Accepted for publication in *Journal of Hydrometeorology*. DOI 10.1175/JHM-D-20-0142.1.

Foufoula-Georgiou 2013). The temporal resolution at which many geochemical tracers are collected, a result of analytical or logistical cost or the need to aggregate them in time to achieve a measurable signal due to low tracer concentrations, contrasts with the time steps typical of many hydrometeorological models (Rosa et al. 2012, Gupta et al. 2020). Accordingly, a method is needed to generate higher frequency datasets of precipitation chemistry from low frequency collections.

Statistical downscaling leverages relationships observed in both fine- and coarse-scale measurements to predict fine-scale variations where only coarse-scale data are available (Ebtehaj and Foufoula-Georgiou 2013, Goncu and Albek 2016). Extensive work has focused on downscaling precipitation rate, including through use of temporal neural networks (e.g. Coulibaly et al. 2005), stochastic methods (e.g. Bordoy and Burlando 2013, D'Onofrio 2013, Poduje and Haberlandt 2017), and conditional multivariate statistical models (e.g. Yang et al. 2010). However, past studies have not temporally downscaled precipitation chemistry data, as is warranted for tracer applications.

Precipitation stable isotope ratios (δ^2H and $\delta^{18}O$) are an ideal test case for developing a downscaling method that can benefit tracer applications, if the downscaling can preserve multi-scale statistical properties (Ebtehaj and Foufoula-Georgiou 2013). Not only is such downscaling in demand, decades of research demonstrate patterns in precipitation isotope ratios that could be leveraged in downscaling; specifically, precipitation amount often covaries with isotopic composition, attributable to the interplay of diverse climatological, physiographical, and meteorological factors in the evaporation, condensation, and transport of atmospheric moisture (e.g. Aggarwal et al. 2016, Aggarwal et al. 2012, Bowen et al. 2019, Ingraham 1998, Konecky et al. 2019, Lee and Fung 2008, Moore et al. 2016, Risi et al. 2008, West et al. 2010). This (typically

77 inverse) covariation between precipitation rates and isotope ratios, often referred to as an "amount
78 effect", represents partially systematic variations at sub-seasonal, monthly, and event time scales
79 (Celle-Jeanton et al. 2001, Conroy et al. 2016, Craig 1961, Craig and Gordon 1965, Gat 1996, Lee
80 and Fung 2008, Moore et al. 2013, Tharammal et al. 2017). If these amount effects share statistical
81 similarities across various time scales, they could support downscaling methods to predict short-
82 term fluctuations. Hypothetically, relationships inferred from sporadic or brief datasets could be
83 used to predict short term variations in precipitation isotopic composition. Those patterns could be
84 superimposed on the longer timescale seasonal patterns, which tend to follow regional patterns
85 (Bowen et al. 2019, Dansgaard 1964, Feng et al. 2009, Allen et al. 2019), to potentially generate
86 realistic, continuous, high-frequency time series of precipitation isotope ratios.

87 In this study, we developed and evaluated a downscaling method that uses the statistical
88 structure of observed stable isotope time series to downscale and generate stable isotope time series
89 at finer resolutions. We used daily observations of precipitation amounts and isotope ratios from
90 27 monitoring stations across the globe. The daily data were artificially aggregated to weekly,
91 biweekly and monthly scales, using amount-weighted running means to simulate coarser-scale
92 datasets on which to apply the method. These aggregated time series were evaluated for statistical
93 trends, specifically characterizing how the time-series means, standard deviations and correlation
94 structures changed as the temporal sampling interval increased. Then, the statistical downscaling
95 method was applied on each of the weekly, biweekly and monthly aggregated tracer time series to
96 generate downscaled tracer values. An ensemble of downscaled realizations was generated at each
97 site, the statistics of which were compared to those of the original daily observations. Our objective
98 was to generate downscaled realizations that accurately preserved the observed daily δ^2H and $\delta^{18}O$

means and standard deviations and the correlation structure between precipitation amount, δ^2H, and $\delta^{18}O$, so that these realizations could be suitable for various potential modeling applications.

2. Data and Methods

a. Site Information and Tracer Datasets

Daily precipitation stable water isotope time series were downloaded from the International Atomic Energy's (IAEA) Global Network of Isotopes in Precipitation (GNIP) and Water Isotope System of Data Analysis, Visualization and Electronic Retrieval (WISER) database (IAEA/WMO 2020). Each time series was filtered to ensure precipitation values were greater than zero and had corresponding δ^2H and $\delta^{18}O$ isotope ratios. All time series with greater than one year of observations were selected, resulting in the 27 datasets used in the subsequent analysis; details pertaining to each site are included in Table S1 located in the *Supplementary Materials*. A minimum time series length of one year was chosen because we wanted to account for site-specific seasonal precipitation patterns in the generated downscaled tracer time series. We acknowledge seasonality is usually characterized over time scales greater than one year, however for this analysis we decided on a minimum of one year so the downscaling method could be applied to as many datasets as possible. In the *Discussion*, the downscaling method's performance was evaluated against the number of years represented in the time series and the frequency of collection, i.e. the number of recorded precipitation events divided by the total number of days represented in the time series. The time series lengths ranged from 1.22 to 15.94 years, with an average of 5.34 years. The total number of samples in a time series ranged from 33 to 1026, with an average of ~210. The site with 33 samples (Barasat, Kolkata; Table S1) was sampled over 1.33 years.

All hydrogen and oxygen isotope ratios of precipitation were denoted as δ^2H and $\delta^{18}O$, defined by

$$\delta\ (‰) = \frac{R_{sample} - R_{std}}{R_{std}}\ 1000 \qquad \text{Eq. 1}$$

where δ was the isotope ratio in delta notation, R_{sample} was the ratio of concentrations between the rare and abundant isotopologues, and R_{std} was the isotopic ratio standard; for this analysis, that standard was the Vienna Standard Mean Ocean Water (VSMOW). The site locations and average stable water isotope observations were represented in Figure 1. The 27 sites have an average mean (+/- standard deviation) daily observed precipitation of 22.80 (21.38) mm, δ^2H of -37.77 (24.62) ‰ and $\delta^{18}O$ of -6.03 (3.21) ‰. The maximum recorded total daily precipitation ranged from 43.0 to 317.5 mm across sites. At the 27 sites, the observed isotope ratios ranged from -228.0 to 43.35 ‰ for δ^2H and -30.50 to 8.81 ‰ for $\delta^{18}O$. The site list included geographic locations across different climates and with uniform and seasonally varying precipitation amounts.

Isotope ratios are often evaluated relative to the Global Meteoric Water Line (GMWL), which is defined as $\delta^2H = 8\delta^{18}O + 10$ ‰ (Craig, 1961). Deuterium excess (*d*-excess $(‰) = \delta^2H - 8\delta^{18}O$) measures the deviation of a water sample's composition from the GMWL (Dansgaard, 1964) and is a useful secondary tracer in that it varies with respect to the evaporation and mixing history of airmasses (e.g., Benetti et al. 2014, Fröhlich et al. 2002, Pfahl and Sodemann 2014). One can use *d*-excess to understand both the source of precipitation and the evolution of moisture during transport (Fröhlich et al. 2002, Good et al. 2014). We aimed to preserve a site's *d*-excess in the downscaled time series because it can be informative for a variety of hydrological and meteorological applications.

145

146 *b. Constructing Low-resolution Datasets*

147 We aggregated each of the 27 GNIP site's datasets using a moving, precipitation amount-
148 weighted average (Eq. 2). This provided us with datasets of low-resolution tracer time series on
149 which to apply the downscaling method to generate downscaled daily estimates to compare with
150 the observed daily values. The precipitation amount-weighted average was defined as

151

152 $$\overline{\delta^2 H_t} = \frac{\sum_{i=1}^{t} P_i \delta^2 H_i}{\sum_{i=1}^{t} P_i} \; and \; \overline{\delta^{18} O_t} = \frac{\sum_{i=1}^{t} P_i \delta^{18} O_i}{\sum_{i=1}^{t} P_i} \qquad \text{Eq. 2}$$

153

154 where P was total precipitation (mm), $\delta^2 H$ (‰) and $\delta^{18} O$ (‰) were the daily observed stable
155 water isotope tracer values at time t (days), and $\overline{\delta^2 H_t}$ (‰) and $\overline{\delta^{18} O_t}$ (‰) were the t-day average
156 tracer value within the specified aggregated temporal interval. $\overline{\delta^2 H_t}$ and $\overline{\delta^{18} O_t}$ values populated
157 a time series at t level of aggregation. We focused on downscaling time series aggregated at t
158 values of 7-, 14-, and 28-days (weekly, biweekly, and monthly).

159 Time series statistics were evaluated across a range of temporal intervals. Moerman et al.
160 (2013) investigated the correlation structure between precipitation amount and $\delta^{18}O$ at Mulu
161 Meteo, Sarawak (Table S1) at daily to 12-week (84-days) time scales. Following their approach,
162 we evaluated trends in the mean (μ), standard deviation (σ), and Pearson correlation coefficient
163 (ρ) at different temporal intervals to capture the time series response and prediction accuracy. The
164 ρ measures the linear correlation between two variables and has a value between -1 and 1, where
165 1 is a total positive linear correlation, 0 is no linear correlation, and -1 is total negative linear
166 correlation. At the daily scale for the 27 GNIP sites, the average (+/- standard deviation) ρ(P, δ^2H)
167 was -0.18 (+/- 0.18), ρ(P, δ^{18}O) was -0.20 (+/- 0.17) and $\rho(\delta^2 H, \delta^{18} O)$ was 0.96 (+/- 0.03).

168

169 *c. Statistical Precipitation Tracer Downscaling Method*

170 1) REMOVAL OF THE DETERMINISTIC TIME SERIES COMPONENT

171 Each aggregated weekly, biweekly and monthly time series (Eq. 2) was treated as an
172 example of a low-resolution dataset on which to apply the downscaling method. We considered
173 each tracer time series to have a deterministic component and a stochastic component. In the first
174 step, the deterministic component was characterized by the seasonality in the precipitation signal
175 and was removed from each set of observations. Isotope ratios in precipitation frequently have
176 been observed to exhibit distinct seasonal signals. These can be approximated as a combination of
177 sinusoidal functions through Fourier decomposition (Allen et al. 2018, Allen et al. 2019, Dutton
178 et al. 2005, Feng et al. 2009, Halder et al. 2015, Vachon et al. 2007, Wilkinson and Ivany 2002).
179 Sinusoidal functions effectively describe the collinear structure and fluctuations in the covariation
180 of δ^2H and δ^{18}O relative to the GMWL (Figure 1; Allen et al. 2018, Craig 1961, Dansgaard 1964).
181 The sine curve parameters (amplitude, phase, and offset) are often predictable in space (Allen et
182 al. 2018, Jasechko et al. 2016) and succinctly represent temporal dynamics because they express
183 continuous, cyclic time series. Allen et al. (2019) used monthly isotopes in precipitation GNIP
184 datasets from across the globe to capture patterns in the precipitation isotope seasonality using
185 sinusoidal functions. When predicting the isotope seasonality, the values of the sine parameters
186 can be described as functions of climate and geography. Additionally, sine curves are useful when
187 describing the propagation of cyclic signals, this has been done to infer catchment-scale mixing
188 processes using the dampening ratio of seasonal isotope amplitudes in streamflow versus
189 precipitation (Kirchner 2016a, 2016b; also see Clow et al. 2018, von Freyberg et al. 2018, Gallart
190 et al. 2020, Jacobs et al. 2018, Jasechko et al. 2016, Lutz et al. 2018, Song et al. 2017).

We fitted sinusoidal functions to each of the site's daily to 12-week aggregated time series to describe the deterministic components using a non-linear, least squares fitting routine, "curve_fit" in Python's (v3.7.6) SciPy Library (v1.2.1), following the methods from Allen et al. (2018). We used a time-weighted fit routine (i.e., not amount weighted and each daily sample had equal weight) to approximate the parameters of the sinusoidal function (Eq. 3) because our ultimate goal related to predicting daily precipitation variations in isotopic composition, regardless of whether or not they are associated with larger events. The sine functions were defined with a fixed period of one year and

$$Precipitation\ \delta^2H \text{ or } \delta^{18}O(f) = A\,sin(2\pi f - \phi) + b, \quad \text{Eq. 3}$$

where f was the fractional year and b was an offset parameter (Allen et al. 2018). All fitted amplitudes (A) and phases (ϕ) were bounded so the amplitude values were positive and the phase ranged between $-\pi$ and π. The presence of large seasonal isotope cycles enables the quantification of mixing, transport and turnover of water in landscape and/or biota. Amplitude dampening reflects mixing processes, phase shifts reflect advective travel times and offset differences reflect proportional contributions of different seasons' precipitation (Kirchner 2016a, 2016b). The defined sinusoidal functions were subtracted from the daily to 12-week aggregated series, thus removing the deterministic time series components.

2) GENERATION OF STOCHASTIC TRACER REALIZATIONS

Next, the daily statistics of the stochastic hydrogen (δ^2H^*) and oxygen ($\delta^{18}O^*$) isotope time series were estimated by using the relationship between the observed daily stochastic statistics

and the stochastic signal's statistics across a range of aggregation intervals (t) multiplied by each site's specific precipitation frequency (λ; defined as the number of days with precipitation divided by the total number of days in a time series). The statistics of the stochastic signal at aggregation interval *t* were denoted with * as μ_t^*, σ_t^*, and ρ_t^* and estimates of these at the daily (*t*=1) resolution were denoted as $\hat{\mu}_1^*, \hat{\sigma}_1^*$, and $\hat{\rho}_1^*$. After removal of the deterministic component, the stochastic signals had mean isotope values of approximately zero across all ranges of $t\lambda$ (Figure 2.a,b). Consequently, we assumed the stochastic signal to behave as a purely random mean zero process ($\hat{\mu}_1^* = 0$), which was further substantiated using tests for independence, autocorrelation, and normality on the stochastic signal (refer to *Sections 2.d* and *3.d*).

The time series standard deviations were greatest at daily time scales and decreased with increasing $t\lambda$ as a power law function (Figure 2.c,d). This decrease resulted from the averaging and weighting of individual daily tracer concentrations by precipitation amounts over longer temporal intervals. By the Central Limit Theorem and the Law of Large Numbers, as the sampling size increases, the sampling distribution converges to a normal distribution where the standard deviation decreases at a rate of $1/n^{0.5}$, where *n* is a number of samples. It should be noted, the results from the Central Limit Theorem and the Law of Large Numbers holds as long as the signal is purely stochastic and there are no trends or heteroscedasticity in the time series. It was assumed a similar relationship was held between the daily standard deviation of days with precipitation tracer values ($\sigma_1^*, ‰$) and the series of known *t*-day aggregation intervals (days) with their corresponding standard deviations in time ($\sigma_t^*, ‰$). $t\lambda$ estimated the expected number of precipitation events in each aggregation level because precipitation does not occur every day (e.g. $n \approx t\lambda$). We expressed this relationship as

237 $$\sigma_t^* = \frac{\hat{\sigma}_1^*}{(t\lambda)^a}, \qquad \text{Eq. 4}$$

238

239 where a is a site-specific parameter defining the rate decrease in σ_t^* with increasing t. We used the
240 non-linear, least-squares fitting routine, "curve_fit", in Python's (v3.7.6) SciPy Library (v1.2.1) to
241 estimate the a and $\hat{\sigma}_1^*$ parameters in Eq. 4. a was constrained between 0.2 and 0.5 in order to
242 bound the curve fitting routine. When $\hat{\sigma}_1^*$ was compared with σ_1^*, a values below 0.2 often
243 underpredicted $\hat{\sigma}_1^*$ and above 0.5 often overpredicted $\hat{\sigma}_1^*$. The initial value predicted for a was set
244 at 0.3, however varying this had negligible influence on the final a parameter estimates and the a
245 parameter estimates were not strongly related to observed standard deviation (for δ^2H^* and $\delta^{18}O^*$
246 $R^2 < 0.002$ and p-value > 0.75). To estimate the daily standard deviation at a site with a biweekly
247 (t = 14) sampling frequency, first λ must be calculated and the time series can be aggregated to
248 28-, 42-, 56-, 70-, and 84-day intervals (Eq. 2) for 2t to 6t, giving 6 points to fit Eq. 4. Weekly time
249 series were aggregated from 2t to 12t (12 points), while monthly time series were aggregated from
250 2t to 3t (3 points). This quantified the decrease in σ_t^* from the available data resolution out to 12
251 weeks (84-days), and allows a and $\hat{\sigma}_1^*$ to be estimated.

252 The ratio of ρ_t^* divided by ρ_1^* across λt was relatively invariant and centered around one
253 (Figure 2.e-g). Thus, Pearson correlation coefficients at a t-day aggregation interval (ρ_t^*) were used
254 to describe the daily correlations ($\hat{\rho}_1^*$) between precipitation amount and the stochastic signal's
255 δ^2H^* and $\delta^{18}O^*$ values.

256 Pseudo-random numbers were generated using a Gaussian copula (Sklar 1959), defined by
257 the estimated daily statistics, $\hat{\mu}_1^*$'s, $\hat{\sigma}_1^*$'s, and $\hat{\rho}_1^*$'s, and conditioned on the observed daily
258 precipitation amounts. Other copula families are possible (e.g. Archimedean copula, Gumbel
259 copula); however, here the Gaussian copula was used because it offered a simple approach for

modeling the dependence of multivariate states (Schneider and Ramos 2014). In probability theory and statistics, the marginal distribution of a subset of a collection of random variables is the probability distribution of one random variable without any reference to other random variables. Copula models separate the dependency structure of multiple random variables from their marginal distributions by mapping each variable through its cumulative distribution functions (CDF) to the unit interval (i.e. closed interval [0,1]). This captures the dependence between the variables using a copula or coupling term, allowing a different marginal distribution for each variable while capturing the multivariate dependencies (Schneider and Ramos 2014, Sklar 1959). Here, a copula captured the multivariate dependencies between precipitation amount, $\delta^2\mathrm{H}^*$ and $\delta^{18}\mathrm{O}^*$. Refer to *Supplemental Material* for further detail on the definition of the Gaussian copula used here. Models using copula techniques have captured the spatial and temporal patterns of precipitation characteristics (Kuhn et al. 2007, Gao et al. 2018), temporally downscale precipitation datasets (Gyasi-Agyei 2011, So et al. 2017), to forecast precipitation events (Bárdossy and Pegram 2009, Khedun 2014) and across other hydrological disciplines (e.g. temperature and rainfall dynamics (Cong and Brady 2012, Schölzel and Friederichs 2008), extreme-value stochastic rainfall events (Kuhn et al. 2007, Laux et al. 2011, Huang et al. 2012), drought distributions from monthly rainfall (Laux et al. 2009), hydraulic conductivity of aquifer systems (Haslauer et al. 2012), and groundwater recharge from precipitation events (Jasechko and Taylor 2015).

For each observed precipitation amount, values of $\delta^2\mathrm{H}^*$ and $\delta^{18}\mathrm{O}^*$ (a 2-number sample representing the stochastic signal) were drawn from a multivariate Gaussian distribution using Python's (v3.7.6) SciPy Library (v1.2.1) with parameters described by $\hat{\rho}_1^*(P, \delta^2 H^*)$, $\hat{\rho}_1^*(P, \delta^{18} O^*)$ and $\hat{\rho}_1^*(\delta^2 H^*, \delta^{18} O^*)$ (refer to Eq. 9 and 10 in the *Supplemental Material*). The covariates used here were precipitation amount and its isotopic composition, however it should be

noted the covariates can change depending on the method's application and data availability. Next, Gaussian CDF values were calculated for each of the generated series. The resulting uniform values were then used to resample from the coarse resolution empirical distribution of isotope ratios for each site, formed by the deseasonalized time series. Each of these values was then rescaled by $\hat{\sigma}_1^*/\sigma_t^*$. The resulting stochastic time series were daily $\delta^2\mathrm{H}^*$ and $\delta^{18}\mathrm{O}^*$ values conditioned on observed precipitation amounts with means of zero, standard deviations of $\hat{\sigma}_1^*$ and Pearson correlation coefficients of $\hat{\rho}_1^*$.

3) FULL SYNTHETIC TIME SERIES GENERATION

The deterministic component, the sinusoidal function from Eq. 3, was added to each generated stochastic time series. The result was a downscaled tracer time series which captured site-specific daily precipitation amount effects, seasonal signals and stochastic variability. Finally, we applied a residual correction on the downscaled synthetic series to preserve the observed aggregated weighted tracer values. For each synthetic value within each aggregation interval, an interval-specific, single correction factor was subtracted from the downscaled values so that there was no difference between that period's downscaled synthetic values aggregated for that interval and the observed coarse-resolution interval's value. In doing so, the precipitation-weighted values of the synthetic time series then equaled the known aggregated value. This property is particularly important as it closes the tracer mass balance. The statistical downscaling method applied to a dataset with a biweekly sampling frequency was summarized and visualized in *Section (ii)* of the *Supplemental Material*.

d. Evaluation of Precipitation Tracer Downscaling Mythology

306 The statistical method was iterated over 100 times generating an ensemble of downscaled
307 isotope time series at each of the 27 GNIP locations. The large number of time series generated
308 for each ensemble allowed for us to quantify the performance of the downscaling method. Each
309 ensemble was expected to capture the observed site-specific tracer means and standard deviations
310 and the correlation coefficients between precipitation amount, δ^2H and $\delta^{18}O$. The statistical
311 downscaling method was evaluated using multiple techniques, detailed in the subsequent
312 paragraphs.

313 After removing the deterministic components, the stochastic time series were expected to
314 have means of approximately zero, a predicable decrease in standard deviation (Eq. 4) and Pearson
315 correlation coefficients at low temporal resolutions appropriately defining daily covariate
316 structures. To test this, σ_1^* and ρ_1^* of the observed datasets were compared to $\hat{\sigma}_1^*$ and $\hat{\rho}_1^*$ of
317 downscaled ensembles using root-mean squared error (RMSE), mean bias error (MBE), and R-
318 squared (R^2). Autocorrelations with lags ranging from 1- to 20-days (Figure 6, refer to *Section 3.c*)
319 and tests for normality were calculated for the stochastic signal of the observed datasets and
320 downscaled ensembles.

321 The average of ensemble means ($\overline{\hat{\mu}_1}$) and standard deviations ($\overline{\hat{\sigma}_1}$) for each isotope ratio
322 and the Pearson correlation coefficients ($\overline{\hat{\rho}_1}$) between precipitation amount and each isotope ratio
323 were compared to the observed daily statistics. R^2 values were calculated for the downscaled
324 ensembles and observed daily site statistics. Each site's observed *d*-excess was evaluated against
325 the downscaled ensemble's *d*-excess. Lastly, we compared the absolute error between the
326 downscaled ensemble and observed time series means to various site-specific and time series
327 characteristics.

328

3. Results

a. Evaluation of Estimated Daily Stochastic Signal Statistics

The estimated daily stochastic signal statistics from weekly, biweekly and monthly aggregation intervals accurately described the observed statistics (Figure 3). The method best predicted $\hat{\sigma}_1^*$ when applied to a weekly series, while the worst approximations of $\hat{\sigma}_1^*$ occurred when it was applied to a monthly series. We expected the weekly time series to best predict $\hat{\sigma}_1^*$ because it better characterizes the change in tracer concentration variance as more values of *t* were used to fit the $\hat{\sigma}_1^*$ and *a* parameters in Eq. 4. For all 27 GNIP sites, the δ^2H $\hat{\sigma}_1^*$ had RMSEs of 2.73 ‰ (MBE = -1.92 ‰) for a weekly series, 5.21 ‰ (MBE = -3.72 ‰) for a biweekly series, and 7.83 ‰ (MBE = -6.02 ‰) for a monthly series. The δ^{18}O $\hat{\sigma}_1^*$ had RMSEs of 0.35 ‰ (MBE = -0.77 ‰) for a weekly series, 0.64 ‰ (MBE = -0.48 ‰) for a biweekly series, and 0.98 ‰ (MBE = -0.24 ‰) for a monthly series. For weekly, biweekly and monthly series, $\hat{\rho}_1^*$(P, δ^2H), $\hat{\rho}_1^*$(P, δ^{18}O), and $\hat{\rho}_1^*$(δ^2H, δ^{18}O) had low RMSEs ranging from 0.01 to 0.18 ‰ and MBEs ranging from -0.01 to 0.03 ‰ across all sites. $\hat{\rho}_1^*$(P, δ^2H) and $\hat{\rho}_1^*$(P, δ^{18}O) were more likely to be overestimated for sites with ρ_1^*(P, δ^2H) and ρ_1^*(P, δ^{18}O) near zero, most likely a result of a site's weak amount effect that can become less significant and sometimes positive as a time series is aggregated. More data could improve estimates of $\hat{\rho}_1^*$. The *Discussion* provides further detail on methods for potentially improving statistical estimates at sites where errors were more apparent.

b. Evaluation of the Downscaled Tracer Realizations

The average of each ensemble's means ($\overline{\hat{\mu}_1}$) and standard deviations ($\overline{\hat{\sigma}_1}$) for each isotope ratio and the Pearson correlation coefficients ($\overline{\hat{\rho}_1}$) between precipitation amount and its corresponding isotope ratios were compared to the observed daily statistics at each site before

applying the residual correction (Figure 4). The downscaled time series with the most accurate $\overline{\hat{\rho}_1}$ were calculated when the method was applied to a weekly time series. After applying a residual correction on each realization in an ensemble, the residual corrected downscaled series accurately captured the μ_1, σ_1, and ρ_1 (Figure 5), though slightly altered R^2 values. The R^2 between μ_1 and $\overline{\hat{\mu}_1}$ and σ_1 and $\overline{\hat{\sigma}_1}$ were similar for the original downscaled (Figure 4.a-d) and residual corrected ensembles (Figure 5.a-d). The residual correction increases the R^2 between ρ_1 and $\overline{\hat{\rho}_1}$ (Figure 4.e-g, Figure 5.e-g), especially when it is applied on a downscaled weekly series. For a downscaled weekly series, the R^2 of $\rho_1(P, \delta^2H)$ and $\overline{\hat{\rho}_1}(P, \delta^2H)$ and $\rho_1(P, \delta^{18}O)$ and $\overline{\hat{\rho}_1}(P, \delta^{18}O)$ increased from 0.88 to 0.93 with a residual correction. For applications where model outputs are directly compared to observation datasets, a residual correction should be applied to generate tracer ensembles which are comparable to the coarser resolution observed values. The average bias between the downscaled and observed time series means and standard deviations were summarized in Table 1. The residual correction on the downscaled ensembles reduced bias in the standard deviations, but had little effect on the means. The *Discussion* provides further detail on potential methods for adding informative covariates (e.g. air temperature) to the downscaled time series estimates at sites where errors were more apparent.

c. Conserved Processes with the Method

An analysis of the observed time series demonstrates strong autocorrelation; when the seasonal signal is removed, the observed autocorrelation is nearly all removed (Figure 6). In fact, the median autocorrelation of the observed time series stochastic signals falls below 5 % after 3-day lags and are approximately zero at 4-day lags, supporting the assumption that the sinusoidal function adequately described the deterministic component and the residual was stationary (i.e.

white noise). The Shapiro-Wilk and the D'Agostino's K^2 normality tests suggest that we could not reject the assumption of normality in the weekly, biweekly and monthly time series (p-value > 0.05). Histograms of the stochastic signals for both isotope ratios across all 27 sites are provided in the *Supplemental Materials* (Figure S3). Next, we calculated autocorrelations from 1- to 20-day lags of the residual corrected downscaled ensembles. The autocorrelations mimicked the observed temporal trends and memory of the daily time series. Autocorrelations for δ^2H and δ^2H^* (Figure 6) and are highly correlated with trends observed in the autocorrelations for $\delta^{18}O$ and $\delta^{18}O^*$ (refer to *Supplemental Materials,* Figure S4). Based on the results from the autocorrelation analysis and normality tests, we concluded the addition of the seasonal signal to the generated stochastic time series captured the large majority of the observed tracer memory in the system.

The means and standard deviations in *d*-excess were accurately captured in the resulting downscaled time series (Figure 7). At each site, *d*-excess was calculated for the observed daily series and each ensemble from the downscaled weekly, biweekly and monthly time scales. The downscaled *d*-excess was over-estimated for the three sites with lowest observed *d*-excess, indicating potential effects to the downscaling method's performance when precipitation is predominantly composed of evaporated waters. These *d*-excess estimates provide a metric for evaluating the downscaled series relative to the GMWL and increases the applicability of this method for tracing meteorological forcing variables and their constituents through modeling environments. Alternative downscaling approaches that independently model δ^2H and $\delta^{18}O$ may not preserve *d*-excess signals and thus would provide precipitation predictions that should not be used in simulations that leverage the information provided by dual-isotope analyses.

4. Discussion

a. Method Evaluation for Select Site Characteristics

We compared the absolute error, calculated by taking the absolute value of the mean of the downscaled ensembles minus the observed mean, to the site's latitude, calculated rainfall frequency (λ), and total length of the time series in years (Figure 8). The largest absolute errors of the mean resulted from downscaling calculations that used monthly aggregated data, yielding average (+/- standard deviation) absolute errors of 2.26 ‰ (2.54 ‰) for δ^2H and 0.33 ‰ (0.35 ‰) for δ^{18}O. Linear regressions between site latitude and absolute errors in the means (derived from monthly, biweekly, and weekly ensembles) showed no strong correlations, suggesting that performance may be partially climate independent (Figure 8). Absolute errors were also not related to the strength of the seasonal isotopic variation, nor were they related to the overall variability in isotopic composition (as quantified by the standard deviation; Figure 9). Alternatively, a weak, but significant relationship was observed between absolute error and λ ($R^2 = 0.25$ and p-value = 0.0001 for δ^2H, $R^2 = 0.23$ and p-value = 0.0002 for δ^{18}O) and average recorded precipitation amount ($R^2 = 0.12$ and p-value = 0.009 for δ^2H, $R^2 = 0.13$ and p-value = 0.0003 for δ^{18}O) for downscaled weekly ensembles, but not for downscaled biweekly or monthly ensembles (Figures 8 and 9). Although not a site characteristic, time-series length significantly influenced absolute errors of downscaled biweekly and monthly ensembles. Longer time series spanning many years support better accounting for interannual variability and removing potential biases towards certain seasons. Nonlinear effects (e.g., continentality (Dansgaard 1964, Rozanski et al., 1993)) may be contributing to relatively high absolute errors, especially at the subtropics and mid-latitudes (Figure 8.a-b). When applying the downscaling method to datasets from these regions, one can adapt the copula framework to account for other influential site-specific characteristics (refer to *Section 2.b)*.

421

422 *b. Method Adaptation for Broader Applications*

423 In this study, weekly, biweekly, and monthly data were used to generate daily observations,
424 but more sophisticated applications could potentially be supported by different datasets. As a
425 general rule, the deterministic time series component can be more accurately estimated with
426 increased tracer sampling frequencies (Figure 8.c-d) and samples collected over longer time frames
427 (Figure 8.e-f). Accurately representing the deterministic component increases the likelihood of a
428 downscaled synthetic time series effectively representing the underlying seasonal patterns and
429 interannual variability at a site. Depending on the application, one may increase or decrease the
430 temporal downscaling intervals beyond daily or 12-week timescales. While not evaluated in this
431 study, one could predict sub-daily datasets with appropriate observation datasets or known
432 statistical properties (i.e., mean, standard deviation, covariance structure of precipitation and its
433 tracer composition) of a site at sub-daily scales (e.g., diurnal cycle).

434 Theoretically, the downscaling methods used in this study can be expanded to higher
435 dimensions and account for other tracer covariates including site conditions such as air temperature
436 and relative humidity. At sites where the method under or overestimates the site statistics, other
437 meteorological variables, such as air temperature, may correlate more strongly with isotope signals
438 than precipitation amount. To do this, one needs to increase the number of covariates accounted
439 for and the matrix dimensions within the copula framework (refer to *Supplemental Materials (i)*
440 *Definition of a Gaussian Copula)*. In these instances, adding more known dimensions to Equations
441 6 and 7 will incorporate additive information into the generated downscaled time series. Including
442 additional known covariates within the copula framework may improve the representation of
443 nonlinear effects at sites in the subtropics and mid-latitudes if meteorological variables (e.g.,

444 relative humidity, air temperature) are highly correlated with changes in tracer concentrations
445 (Figures 8.a-b).

446 Not only would a downscaled time series facilitate running more detailed models that
447 improve process understanding, but they also allow for better tracking of uncertainties associated
448 with inferences drawn from those models. We compared the mean of the observed biweekly series
449 and the mean of the downscaled biweekly ensemble aggregated to biweekly time scales using Eq.
450 2. The absolute error of the mean across all sites was 0.90 ‰ for δ^2H and 0.14 ‰ for δ^{18}O. This
451 suggests models using downscaled tracers would mimic temporal trends observed at biweekly time
452 scales, while also tracking processes and uncertainties only discernible at finer time scales. As
453 expected, when the residual corrected downscaled biweekly ensemble was aggregated to biweekly
454 time scales, the absolute error of the mean was approximately zero. To evaluate how the
455 downscaling method compared to a naive downscale with no high-frequency statistical
456 information, we created a daily time series where all precipitation events that occurred within each
457 14-day interval had the same isotopic composition equal to the observed biweekly values. The
458 absolute error of the mean across all sites (+/- standard deviation) was 2.74 ‰ (2.24 ‰) for δ^2H
459 and 0.39 ‰ (0.31 ‰) for δ^{18}O, which was higher than the absolute error of the mean calculated
460 for all the downscaled biweekly ensembles (1.69 ‰ (1.61 ‰) for δ^2H and 0.23 ‰ (0.24 ‰) for
461 δ^{18}O).

462 Due to limited data, all of the above analyses used the entire dataset to calculate the
463 statistics, fit the models and apply the downscaling method. At sites with more than 5 years of
464 data, we used the first 4 years to build a downscaling model to apply on the 5th year's precipitation
465 time series. We generated an ensemble of 100 downscaled δ^2H and δ^{18}O time series at each site
466 and compared it to the observed δ^2H and δ^{18}O from the 5th year of the time series. Based on

training and testing sizes, eight sites were used in this analysis and the absolute error of the mean (+/- standard deviation) for δ^2H was 4.80 ‰ (3.17 ‰), 4.89 ‰ (3.26 ‰) and 5.52 ‰ (3.50 ‰) downscaled from weekly, biweekly, and monthly series, respectively. The absolute error of the mean (+/- standard deviation) for $\delta^{18}O$ was 0.79 ‰ (0.59 ‰), 0.78 ‰ (0.63 ‰) and 0.85 ‰ (0.67 ‰) downscaled from weekly, biweekly, and monthly series, respectively. Based on these promising results, our downscaling method could be built using several years of precipitation data with a known concentration and then applied to years where only precipitation amount is available.

This method can be broadly applied to produce ensembles of downscaled datasets for various geochemical modeling applications. Ensembles decrease the risk of tying conclusions to one specific time series. The downscaled ensembles can be generated using the same statistics (like shown here) or multiple ensembles can be generated with varying statistical properties. Examples of different ensembles include time series generated from downscaled statistics estimated from different aggregation intervals (e.g. weekly and biweekly), employing a non-Gaussian copula framework (e.g. Gumbel copula, Extreme-value copula) to populate a conditioned stochastic signal's time series, and increasing dimensions of the copula framework by including additive meteorological variables (e.g. air temperature). Correspondingly, the geochemical tracer ensembles could be used for model selection and with numerous model and parameter sensitivity and uncertainty analyses. Ensembles could be useful in developing frameworks for model-data fusion by merging observational data with model outputs to improve model quality and characterize its uncertainty.

This downscaling approach could be extended across large spatial extents for use in global isotopic models or empirically based geographic simulations to represent sites with limited or no high-frequency observations available. To do this, one could generate downscaled geochemical

tracers correlating with precipitation inputs at the grid-scale. Lastly, the methodology can be applied to other geochemical tracers for understanding site-specific dynamics (e.g. chemical leaching, sediment transport and loading) or climatological applications (e.g. nitrogen deposition, carbon sequestration).

5. Conclusions

This statistical downscaling method generates datasets that maintain informative site-specific correlation structures between covariates and the geochemical tracer and retains the statistical properties of underlying processes (e.g., *d*-excess, amount effects). By modeling hydrologic dynamics using downscaled tracers, researchers can enhance understanding of physical processes without collecting fine temporal in-situ data. While an individual realization of this downscaling approach may generate reasonable estimates of true high-frequency values, iterating analyses using an ensemble of realizations allows for uncertainties in generated time series to be propagated through subsequent modeling and tracer-based analyses. The method is sufficiently general and can be applied for a variety of applications to generate downscaled ensembles for use in meteorological and hydrometeorological models to evaluate model performance, investigate system processes across spatial scales and is additive to model-data fusion frameworks.

Acknowledgements

The authors acknowledge the support of the United States National Science Foundation (DEB-1802885, DEB-1802880 and AGS-1954660) and thank the anonymous reviewers for their time and effort spent reviewing this manuscript. The authors state no conflict of interest.

Data Availability Statement

Python code is provided in the *Supplemental Material* to generate geochemical synthetic time series based on the user's site-specific time series statistics. The code is intended to be easily adaptable to higher dimensions or other user specific applications. Additional materials can be made available upon request.

REFERENCES

Abbott, B. W., V. Baranov, C. Mendoza-Lera, M. Nikolakopoulou, A. Harjung, T. Kolbe, M. N. Balasubramanian, T. N. Vaessen, F. Ciocca, A. Campeau, M. B. Wallin, P. Romeijn, M. Antonelli, J. Gonçalves, T. Datry, A. M. Laverman, J. de Dreuzy, D. M. Hannah, S. Krause, C. Oldham, and G. Pinay, 2016: Using multi-tracer inference to move beyond single catchment ecohydrology. *Earth-Sci. Rev.*, **160**, 19-42, https://doi.org/10.1016/j.earscirev.2016.06.014.

Aggarwal, P. K., O. A. Alduchov, K. O. Froehlich, L. J. Araguas-Araguas, N. C. Sturchio, and N. Kurita, 2012: Stable isotopes in global precipitation: a unified interpretation based on atmospheric moisture residence time. *Geophys. Res. Lett.,* **39***,* 1-6, https://doi.org/10.1029/2012GL051937.

Aggarwal, P. K., U. Romatschke, L. Araguas-Araguas, D. Belachew, F. J. Longstaffe, P. Berg, C. Schumacher, and A. Funk, 2016: Proportions of convective and stratiform precipitation revealed in water isotope ratios. *Nat. Geosci.*, **9**, 624-629, https://doi.org/10.1038/ngeo2739.

534 Allen, S. T., Jasechko, S., Berghuijs, W. R., Welker, J. M., Goldsmith, G. R., and Kirchner, J. W.,
535 2019: Global sinusoidal seasonality in precipitation isotopes, *Hydrol. Earth Syst. Sci.*, **23**, 3423–
536 3436, https://doi.org/10.5194/hess-23-3423-2019.
537
538 Allen, S. T., Kirchner, J. W., & Goldsmith, G. R., 2018. Predicting spatial patterns in precipitation
539 isotope (δ2H and δ18O) seasonality using sinusoidal isoscapes. *Geophys. Res.*, **45**, 4859–4868,
540 https://doi.org/10.1029/2018GL077458.
541
542 Bailey, A., E. Posmentier, and X. Feng, 2018: Patterns of Evaporation and Precipitation Drive
543 Global Isotopic Changes in Atmospheric Moisture. *Geophy. Res. Lett.*, **45**, 7093-7101,
544 https://doi.org/10.1029/2018GL078254.
545
546 Bárdossy, A. and G. G. S. Pegram, 2009: Copula based multisite model for daily precipitation
547 simulation. *Hydrol. Earth Syst. Sci.,* **13***,* 2299-2314.
548
549 Benetti, M., G. Reverdin, C. Pierre, L. Merlivat, C. Risi, H. C. Steen-Larsen, and F. Vimeux, 2014:
550 Deuterium excess in marine water vapor: Dependency on relative humidity and surface wind speed
551 during evaporation. *J. Geophys. Res-Atmos.*, **119**, 583-593,
552 https://doi.org/10.1002/2013JD020535.
553
554 Brady, E., Stevenson, S., Bailey, D., Liu, Z., Noone, D., Nusbaumer, J., Otto-Bliesner, B.
555 L., Tabor, C., Tomas, R., Wong, T., et al., 2019: The Connected Isotopic Water Cycle in the

Community Earth System Model Version 1. *J. Adv. Model. Earth Syst.*, **11**, 2547– 2566, https://doi.org/10.1029/2019MS001663.

Brooks, J. R., J. J. Gibson, S. J. Birks, M. H. Weber, K. D. Rodecap, and J. L. Stoddard, 2014: Stable isotope estimates of evaporation: inflow and water residence time for lakes across the United States as a tool for national lake water quality assessments. *Limnol. Oceanogr.,* **59**, 2150-2165, https://doi.org/10.4319/lo.2014.59.6.2150.

Bordoy, R. and P. Burlando, 2013: Stochastic downscaling of climate model precipitation outputs in orographically complex regions: 2. Downscaling methodology. *Water Resour. Res.,* **50***,* 562-579, https://doi.org/10.1002/wrcr.20443.

Bowen, G. J., Z. Cai, R. P. Fiorella, and A. L. Putman, 2019: Isotopes in the water cycle: Regional- to global-scale patterns and applications. *Annu. Rev. Earth Planet Sci.*, **47**, 453-479, https://doi.org/10.1146/annurev-earth-053018-060220.

Bowen, G. J. and S. P. Good, 2015: Incorporating water isotopes in hydrological and water resource investigations. *WIREs. Water*, **2**, *2*, 107-119. https://doi.org/10.1002/wat2.1069.

Celle-Jeanton, H. Y. Travi, and B. Blavoux, 2001: Isotopic typology of the precipitation in the Western Mediterranean region at three different time scales. *Geophys. Res. Lett.*, **28**, *7*, 1215-1218, https://doi.org/10.1029/2000GL012407.

Clow, D. W., M. A. Mast, and J. O. Sickman, 2018: Linking transit times to catchment sensitivity to atmospheric deposition of acidity and nitrogen in mountains of the western United States, *Hydrol. Process*, **32**, *16*, 2456–2470, https://doi.org/10.1002/hyp.13183.

Cong, R. and M. Brady, 2012: The interdependence between rainfall and temperature: copula analysis. *The Scientific World Journal,* **2012**, 1-11, https://doi.org/10.1100/2012/405675.

Conroy, J. L., Noone, D., Cobb, K. M., Moerman, J. W., and Konecky, B. L. (2016), Paired stable isotopologues in precipitation and vapor: A case study of the amount effect within western tropical Pacific storms, *J. Geophys. Res. Atmos.*, **121**, 3290– 3303, https://doi.org/10.1002/2015JD023844.

Coulibaly, P., Y. B. Dibike, and F. Anctil, 2005: Downscaling precipitation and temperature with temporal neutral networks. *J. Hydrometeor.,* **6***,* 483-496, https://doi.org/10.1175/JHM409.1.

Craig, H., 1961: Isotopic variations in meteoric waters. *Science*, **133**, 1702-1703.

Craig, H. and L. I. Gordon, 1965: Deuterium and oxygen-18 variations in the ocean and the marine atmosphere. *In E. Tongiorgi, ed*, Proceedings of a Conference on Stable Isotopes in Oceanographic Studies and Paleotemperatures, Spoleto, Italy, pp 9-130.

Dansgaard, W., 1964: Stable isotopes in precipitation. *Tellus*, **16**, 436–468, https://doi.org/10.1111/j.2153-3490.1964.tb00181.x.

D'Onofrio, D. 2014: Stochastic rainfall downscaling of climate models. *J. Hydrometeor.,***15**, 830-843, https://doi.org/10.1175/JHM-D-13-096.1.

Dutton, A., B. H. Wilkinson, J. M. Welker, G. J. Bowen, and K. C. Lohmann, 2005: Spatial distribution and seasonal variation in 18O/16O of modern precipitation and river water across the conterminous USA, *Hydrol. Process.*, **19**, *20*, 4121–4146, https://doi.org/10.1002/hyp.5876.

Ebtehaj, A. M., and E. Foufoula-Georgiou, 2013: On variational downscaling, fusion, and assimilation of hydrometeorological states: A unified framework via regularization. *Water Resour. Res.*, **49**, 5944– 5963, https://doi.org/10.1002/wrcr.20424.

Fekete, B. M., J. J. Gibson, P. Aggarwal, C. J. Vörösmarty, 2006: Application of isotopic tracers in continental scale hydrological modeling. *J. Hydrol.*, **330**, *3-4*, 444-456, https://doi.org/10.1016/j.jhydrol.2006.04.029.

Feng, X., A. M. Faiia, and E. S. Posmentier, 2009: Seasonality of isotopes in precipitation: A global perspective. *J. Geophys. Res-Atmos*, **114**, *D8*, https://doi.org/10.1029/2008JD011279.

v. Freyberg, J., S. T. Allen, S. Seeger, M. Weiler, and J. W. Kirchner, 2018: Sensitivity of young water fractions to hydroclimatic forcing and landscape properties across 22 Swiss catchments, *Hydrol. Earth Syst. Sci.*, 22, *7*, 3841–3861, https://doi.org/10.5194/hess-22-3841-2018.

Fröehlich K., J. J. Gibson, and P. K. Aggarwal, 2002: Deuterium excess in precipitation and its climatological significance. Study of environmental change using isotope techniques. *C&S Papers Series*, **13**, 54-65. International Atomic Energy Agency: Vienna, Austria.

Gallart, F., M. Valiente, P. Llorens, C. Cayuela, M. Sprenger, and J. Latron, 2020: Investigating young water fractions in a small Mediterranean mountain catchment: both precipitation forcing and sampling frequency matter. *Hydrol. Processes*, https://doi.org/10.1002/hyp.13806.

Gao, C., Y. Xu, Q. Zhu, Z. Bai, and L. Liu, 2018: Stochastic generation of daily rainfall events: a single-site rainfall model with copula-based joint simulation of rainfall characteristics and classification and simulation of rainfall patterns. *J. Hydrol,* **564**, 41-58, https://doi.org/10.1016/j.jhydrol.2018.06.073.

Gat, J. R., 1996: Oxygen and hydrogen isotopes in the hydrologic cycle. *Annu. Rev. Earth Planet Sci.*, **24**, 225-262, https://doi.org/10.1146/annurev.earth.24.1.225.

Gibson, J. J., T. W. D. Edwards, S. J. Birks, N. A. St Amour, W. M. Buhay, P. McEachern, B. B. Wolfe, and D. L. Peters, 2005: Progress in isotope tracer hydrology in Canada. *Hydrol. Process.*, **19***, 1*, 303-327, https://doi.org/10.1002/hyp.5766.

Goncu, S., and E. Albek, 2016: Statistical downscaling of meteorological time series and climatic projections in a watershed in Turkey. Theoretical and Applied Climatology, **126,** 1-2, https://link.gale.com/apps/doc/A470736525/AONE?u=s8405248&sid=AONE&xid=e894de9e.

Good S. P., D. V. Mallia, J. C. Lin, and G. J. Bowen, 2014: Stable isotope analysis of precipitation samples obtained via crowdsourcing reveals the spatiotemporal evolution of superstorm sandy. PLOS ONE **9**, *3*, e91117, https://doi.org/10.1371/journal.pone.0091117.

Good, S. P., D. Noone, and G. Bowen, 2015: Hydrologic connectivity constrains partitioning of global terrestrial water fluxes. *Science,* **349***,* 175-177, https://doi.org/10.1126/science.aaa5931.

Gupta, A., E. P. Gerber, and P. H. Lauritzen, 2020: Numerical impacts on tracer transport: A proposed intercomparison test of Atmospheric General Circulation Models. *Q. J. R. Meteorol. Soc.*, **146**, 3937– 3964, https://doi.org/10.1002/qj.3881.

Gyasi-Agyei, Y., 2011: Copula-based daily rainfall disaggregation model. *Water Resour. Res.,* **47***,* W07535, https://doi.org/10.1029/2011WR010519.

Halder, J., S. Terzer, L. I. Wassenaar, L. J. Araguás-Araguás, and P. K. Aggarwal, 2015: The Global Network of Isotopes in Rivers (GNIR): integration of water isotopes in watershed observation and riverine research. *Hydrol. Earth Syst. Sci.*, **19**, *8*, 3419–3431, https://doi.org/10.5194/hess-19-3419-2015.

Haslauer, C. P., P. Guthke, A. Bádossy, and E. A. Sudicky, 2012: Effects of non-gaussian copula-based hydraulic conductivity fields on macrodispersion. *Water Resour. Res.,* **48***,* 1-18, https://doi.org/10.1029/2011WR011425.

Hoffmann, G., J. Jouzel and V. Masson, 2000: Stable water isotopes in atmospheric general circulation models. *Hydrol. Processes,* **14**, 1385-1406, https://doi.org/10.1002/1099-1085(20000615)14:8<1385::AID-HYP989>3.0.CO2-1.

Huang, J., J. Zhang, Z. Zhang, S. Sun and J. Yao, 2012: Simulation of extreme precipitation indices in the Yangtze River basin by using statistical downscaling method (SDSM). *Theor. Appl. Climatol.* **108**, 325–343, https://doi.org/10.1007/s00704-011-0536-3.

IAEA/WMO (2020). Global Network of Isotopes in Precipitation. The GNIP Database. Accessible at: http://www.iaea.org/water.

Ingraham, N. L., 1998: Isotopic variations in precipitation. In C. Kendall & J. J. McDonnell (Eds.), Isotope Tracers in Catchment Hydrology (pp. 87–118). Amsterdam: Elsevier Science, https://doi.org/10.1016/B978-0-444-81546-0.50010-0.

Jacobs, S. R., E. Timbe, B. Weeser, M. C. Rufino, K. Butterbach-Bahl, and L. Breuer, 2018: Assessment of hydrological pathways in East African montane catchments under different land use. *Hydrol. Earth Syst. Sci.*, **22**, 4981-5000, https://doi.org/10.5194/hess-22-4981-2018.

Jasechko, S. and R. Taylor, 2015: Intensive rainfall recharges tropical groundwaters. *Environ. Res. Lett.,* **10***,* https://doi.org/10.1088/1748-9326/10/12/124015.

Jasechko, S., J. W. Kirchner, J. M. Welker, and J. J. McDonnell, 2016: Substantial proportion of global streamflow less than three months old. *Nat. Geosci.*, **9**, *2*, 126–129, https://doi.org/10.1038/ngeo2636.

Kanner, L. C., N. H. Buenning, L. D. Stott, A. Timmermann, and D. Noone, 2014: The role of soil processes in $\delta^{18}O$ terrestrial climate proxies. *Global Biogeochem. Cycles,* **28**, 239-252, https://doi.org/10.1002/2013GB004742.

Kendall, C. and J. J. McDonnell, 2012: *Isotope tracers in catchment hydrology*. Elsevier, 870pp.

Khedun, C. P., A. K. Mishra, V. P. Singh and J. R. Giardino, 2014: A copula-based precipitation forecasting model: investigating the interdecadal modulation of ENSO's impacts on monthly precipitation. *Water Resour. Res.,* **50***,* 580-600, https://doi.org/10.1002/2013WR013763.

Kirchner, J. W., 2016a: Aggregation in environmental systems—Part 1: Seasonal tracer cycles quantify young water fractions, but not mean transit times, in spatially heterogeneous catchments. *Hydrol. Earth Syst. Sci.*, 20, *1*, 279–297, https://doi.org/10.5194/hess-20-279-2016.

Kirchner, J. W., 2016b: Aggregation in environmental systems—Part 2: Catchment mean transit times and young water fractions under hydrologic nonstationarity. *Hydrol. Earth Syst. Sci.*, **20**, *1*, 299–328, https://doi.org/10.5194/hess-20-299-2016.

Konecky, B. L., D. C. Noone, and K. M. Cobb, 2019: The influence of competing hydroclimate processes on stable isotope ratios in tropical rainfall. *Geophys. Res. Lett.*, **46**, 1622-1633, https://doi.org/10.1029/2018GL080188.

Krause, P., D. P. Boyle, and F. Bäse, 2005: Comparison of different efficiency criteria for hydrological model assessment. *Adv. in Geosci.,* **5***,* 89-97, https://doi.org/1680-7359/adgeo/2005-5-89.

Kuhn, G., S. Khan, A. R. Ganguly, and M. L. Branstetter, 2007: Geospatial-temporal dependence among weekly precipitation extremes with applications to observations and climate model simulations in South America. *Adv. Water Resour.,* **30***,* 2401-2423, https://doi.org/10.1016/j.advwatres.2007.05.006.

Laux, P., S. Vogl, W. Qiu, H. R. Knoche, and H. Kunstmann, 2011: Copula-based statistical refinement of precipitation in RCM simulations over complex terrain. *Hydrol. Earth Sys. Sci.,* **15***,* 2401-2419, https://doi.org/10.5194/hess-15-2401-2011.

734 Laux, P., S. Wagner, A. Wagner, J. Jacobeit, A. Bárdossy, and H. Kunstmann, 2009: Modelling
735 daily precipitation features in the Volta Basin of West Africa. *International Journal of*
736 *Climatology,* **29***,* 937-954, https://doi.org/10.1002/joc.1852.
737
738 Lee, J. E. and I. Fung, 2008: "Amount effect" of water isotopes and quantitative analysis of post-
739 condensation processes. *Hydrol. Process*., **22**, 1-8, https://doi.org/10.1002/hyp.6637.
740
741 Lutz, S. R., R. Krieg, C. Müller, M. Zink, K. Knöller, L. Samaniego, and R. Merz, 2018: Spatial
742 patterns of water age: Using young water fractions to improve the characterization of transit times
743 in contrasting catchments. *Water Resour. Res.*, **54**, *7*, 4767–4784,
744 https://doi.org/10.1029/2017WR022216.
745
746 McGuire, K. J. and J. J. McDonnell, 2006: A review and evaluation of catchment transit time
747 modeling. *J. Hydrol.,* **330***,* 543-563, https://doi.org/10.1016/j.jhydrol.2006.04.020.
748
749 Moerman, J. W., K. M. Cobb, J. F., Adkins, H. Sodemann, B. Clark, and A. A. Tuen, 2013: Diurnal
750 to interannual rainfall $\delta^{18}O$ variations in northern Borneo driven by regional hydrology. *Earth*
751 *Planet. Sci. Lett.,* **369-370***,* 108-109, https://doi.org/10.1016/j.epsl.2013.03.014.
752
753 Moore, M., Kuang, Z., and Blossey, P. N., 2014: A moisture budget perspective of the amount
754 effect, *Geophys. Res. Lett*., **41**, 1329– 1335, https://doi.org/10.1002/2013GL058302.
755

Moore, M., P. N. Blossey, A. Muhlbauer, and Z. Kuang, 2016: Microphysical controls on the isotopic composition of wintertime orographic precipitation. *J. Geophys. Res. Atmos.*, **121**, 7235-7253, https://doi.org/10.1002/2015JD023763.

Nusbaumer, J., T. E. Wong, C. Bardeen, and D. Noone, 2017: Evaluating hydrological processes in the Community Atmosphere Model Version 5 (CAM5) using stable isotope ratios of water. *J. Adv. Model Earth Sy.*, **9**, *2*, 949-977, https://doi.org/10.1002/2016MS000839.

Orbe, C., D. Rind, J. Jonas, L. Nazarenko, G. Faluvegi, L. T. Murray, D. T. Shindell, K. Tsigaridis, T. Zhou, M. Kelley, and G. A. Schmidt, 2020: GISS Model E2.2: A climate model optimized for the middle atmosphere—2. Validation of large-scale transport and evaluation of climate response. *J. Geophys. Res. Atmos.*, **125**, https://doi-org.ezproxy.proxy.library.oregonstate.edu/10.1029/2020JD033151.

Pfahl, S. and H. Sodemann, 2014: What controls deuterium excess in global precipitation?. *Clim. Past*, **10**, 771–781, https://doi.org/10.5194/cp-10-771-2014.

Poduje, A. C. C. and U. Haberlandt, 2017: Short time step continuous rainfall modeling and simulation of extreme events. *J. Hydrol.,* **552***,* 182-197, https://doi.org/10.1016/j.jhydrol.2017.06.036.

Remondi, F., J. W. Kircher, P. Burlando, and S. Fatichi, 2018: Water flux tracking with a distributed hydrologic model to quantify controls on the spatio-temporal variability of transit time distributions. *Water Resour. Res.*, **54**, *4*, 3081-3099, https://doi.org/10.1002/2017WR021689.

Risi, C., D. Noone, J. Worden, C. Frankenberg, G. Stiller, M. Kiefer, B. Funke, K. Walker, P. Bernath, M. Schneider, D. Wunch, V. Sherlock, N. Deutscher, D. Griffith, P. O. Wennberg, K. Strong, D. Smale, E. Mahieu, S. Barthlott, F. Hase, O. García, J. Notholt, T. Warneke, G. Toon, D. Sayres, S. Bony, J. Lee, D. Brown, R. Uemura, C. Sturm, 2012: Process-evaluation of tropospheric humidity simulated by general circulation models using water vapor isotopic observations: 2. Using isotopic diagnostics to understand the mid and upper tropospheric moist bias in the tropics and subtropics, *J. Geophys. Res.*, **117**, *D05304*, https://doi.org/10.1029/2011JD016623.

Risi, C., S. Bony, S., and F. Vimeux, 2008: Influence of convective processes on the isotopic composition (δ18O and δD) of precipitation and water vapor in the tropics: 2. Physical interpretation of the amount effect. *J. Geophys. Res.*, **113**, D19306, https://doi.org/10.1029/2008JD009943.

Rosa, D., Lamarque, J. F., and Collins, W. D. 2012: Global transport of passive tracers in conventional and superparameterized climate models: Evaluation of multi-scale methods, *J. Adv. Model. Earth Syst.*, **4**, https://doi.org/10.1029/2012MS000206.

Rozanski, K., Araguás- Araguás, L. and Gonfiantini, R. 1993: Isotopic Patterns in Modern Global Precipitation. *In Climate Change in Continental Isotopic Records* (eds P.K. Swart, K.C. Lohmann, J. Mckenzie and S. Savin). https://doi.org/10.1029/GM078p0001.

Schölzel, C. and P. Friederichs, 2008: Multivariate non-normally distributed random variables in climate research- introduction to the copula approach. *Nonlinear Processes in Geophysics,* **15***,* 761-772. https://doi.org/10.5194/npg-15-761-2008.

Schneider, M. and F. Ramos, 2014: Transductive learning for multi-task copula processes. *Technical Report*, 1-8, http://www-personal.usyd.edu.au/~framos/Publications_files/TransductiveCopulas.pdf.

Sklar, A., 1959: Fonctions de répartition à n dimensions et leurs marges. *Publ. Inst. Stat. Univ. Paris,* **8**, 229–231.

So, B., J. Kim, H. Kwon, and C. H. R. Lima, 2017: Stochastic extreme downscaling model for an assessment of changes in rainfall intensity-duration-frequency curves over South Korea using multiple regional climate models. *J. Hydrol.,* **553**, 321-337, https://doi.org/10.1016/j.hydrol.2017.07.061.

Soderberg, K., S. P. Good, L. Wang, and K. Caylor, 2012: Stable isotopes of water vapor in the vadose zone: a review of measurement and modeling techniques. *Vadose Zone J*, https://doi.org/10.2136/vzj2011.0165.

Song, C., G. Wang, G. Liu, T. Mao, X. Sun, and X. Chen, 2016: Stable isotope variations of precipitation and streamflow reveal the young water fraction of a permafrost watershed. *Hydrol. Processes*, **31**, *4*, 935–947, doi:10.1002/hyp.11077.

Sprenger, M., C. Stumpp, M. Weiler, W. Aeschbach, S. T. Allen, P. Benettin, M. Dubbert, A. Hartmann, M. Hrachowitz, J. W. Kirchner, J. J. McDonnell, N. Orlowski, D. Penna, S. Pfahl, M. Rinderer, N. Rodriquez, M. Schmidt, and C. Werner, 2019: The demographics of water: A review of water ages in the critical zone. *Rev. of Geophysics*, **57**, 800-834, https://doi.org/10.1029/2018RG000633.

Steen-Larsen, H. C., C. Risi, M. Werner, K. Yoshimura, and V. Masson-Delmotte, 2017: Evaluating the skills of isotope-enabled general circulation models against in situ atmospheric water vapor isotope observations, *J. Geophys. Res. Atmos.*, **122**, 246–263, https://doi.org/10.1002/2016JD025443.

Stumpp, C., J. Klaus, and W. Stichler, 2014: Analysis of long-term stable isotopic composition in German precipitation. *J. Hydrol.,* **517**, 351-361, https://doi.org/10.1016/j.jhydrol.2014.05.034.

Stumpp, C., W. Stichler, M. Kandolf, and J. Šimunek, 2012: Effects of land cover and fertilization method on water flow and solute transport in five lysimeters: a long-term study using stable water isotopes. *Vadose Zone J.,* https://doi.org/10.2136/vzj2011.0075.

Tharammal, T., Bala, G., and Noone, D., 2017: Impact of deep convection on the isotopic amount effect in tropical precipitation, *J. Geophys. Res. Atmos.*, **122**, 1505– 1523, http://dx.doi.org/10.1002/2016JD025555.

Turnadge, C. and B. D. Smerdon, 2014: A review of methods for modelling environmental tracers in groundwater: Advantages of tracer concentration simulation. *J. Hydrol.*, **519**, http://dx.doi.org/10.1016/j.jhydrol.2014.10.056.

Vachon, R. W., J. W. C. White, E. Gutmann, and J. M. Welker, 2007: Amount-weighted annual isotopic (δ18O) values are affected by the seasonality of precipitation: A sensitivity study. *Geophys. Res. Lett.*, **34**, *21*, L21707, doi:10.1029/2007GL030547.

West, J. B., G. J. Bowen, T. E. Dawson, and K. P. Tu, 2010: *Isoscapes: Understanding movement, pattern, and process on Earth through isotope mapping*. Springer, 487pp.

Wiederhold, J. G., 2015: Metal stable isotope signatures as tracers in environmental geochemistry. *Environ. Sci. Technol.*, **49**, 2606-2624, https://doi.org/10.1021/es504683e.

Wilkinson, B. H. and L. C. Ivany, 2002: Paleoclimatic inference from stable isotope profiles of accretionary biogenic hardparts – a quantitative approach to the evaluation of incomplete data, *Palaeogeogr. Palaeoclimatol. Palaeoecol.*, **185**, *1*, 95–114, https://doi.org/10.1016/S0031-0182(02)00279-1.

868 Wong, T. E., J. Nusbaumer, and D. C. Noone, 2017: Evaluation of modeled land-atmosphere
869 exchanges with a comprehensive water isotope fractionation scheme in version 4 of the
870 Community Land Model. *J. Adv. Model Earth Sy.*, **9**, *2*, 978-1001,
871 https://doi.org/10.1002/2016MS000842.

872

873 Yang, W., A. Bárdossy, and H. J. Caspary, 2010: Downscaling daily precipitation time series
874 using a combined circulation- and regression-based approach. *Theor. Appl. Climatol*, **102**, 439-
875 454, https://doi.org/10.1007/s00704-010-0272-0.

876

877 # TABLES

878 Table 1. Average bias (predicted - observed statistic) (+/- standard deviation) for downscaled and
879 *residual corrected downscaled* ensembles

	Bias in the Means (‰)				**Bias in the Standard Deviations (‰)**			
	δ^2H	***δ^2H***	**δ^{18}O**	***$\delta^{18}O$***	**δ^2H**	***δ^2H***	**δ^{18}O**	***$\delta^{18}O$***
Weekly	-0.10 (1.39)	*0.01 (1.79)*	-0.02 (0.20)	*-0.03 (0.26)*	0.02 (2.38)	*1.95 (3.30)*	0.004 (0.34)	*0.25 (0.46)*
Biweekly	-1.00 (2.20)	*-0.68 (3.50)*	-0.16 (0.30)	*-0.12 (0.46)*	1.04 (3.95)	*2.76 (4.14)*	0.17 (0.56)	*0.39 (0.59)*
Monthly	-1.43 (3.08)	*-0.13 (5.86)*	-0.23 (0.43)	*-0.05 (0.74)*	2.20 (8.75)	*3.28 (8.81)*	0.28 (1.12)	*0.43 (1.12)*

880

881 # FIGURES

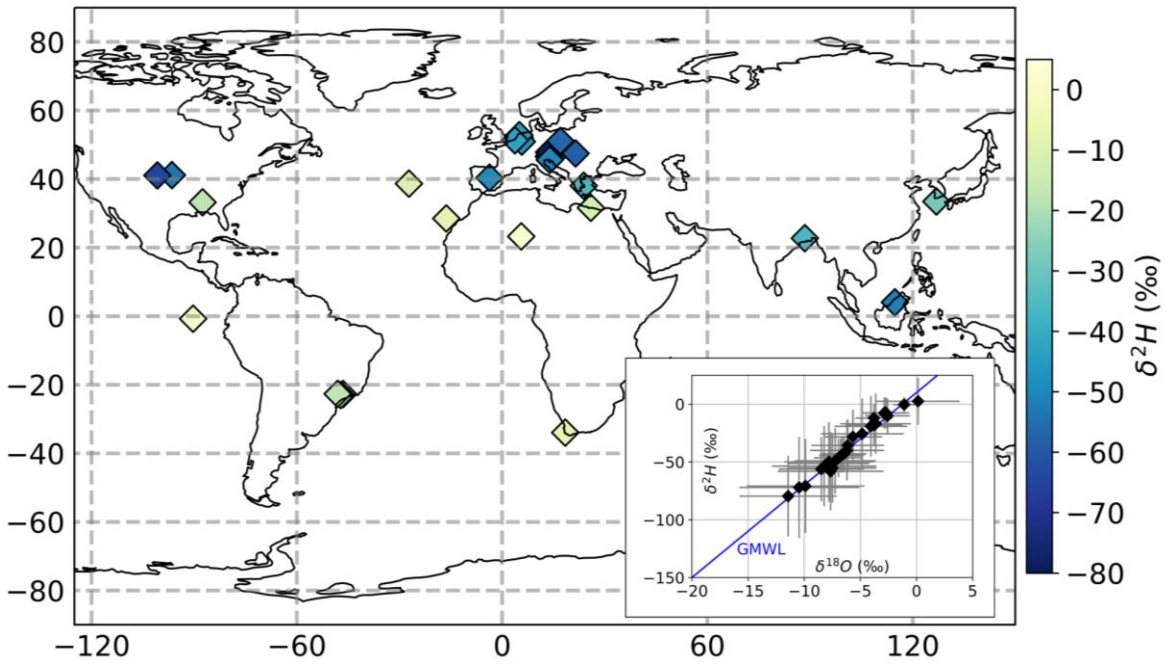

882

883 Figure 1. The large map displays the 27 GNIP site locations and their average $\boldsymbol{\delta^2H}$ precipitation
884 measurements. The smaller figure is a dual isotope plot with the mean and standard deviations of
885 all daily precipitation stable water isotope measurements (δ^2H, $\delta^{18}O$) at the 27 GNIP sites. The
886 Global Meteoric Water Line (GMWL) is included in the subplot. Refer to Table S1 in the
887 *Supplemental Material* for more site-specific characteristics.

888

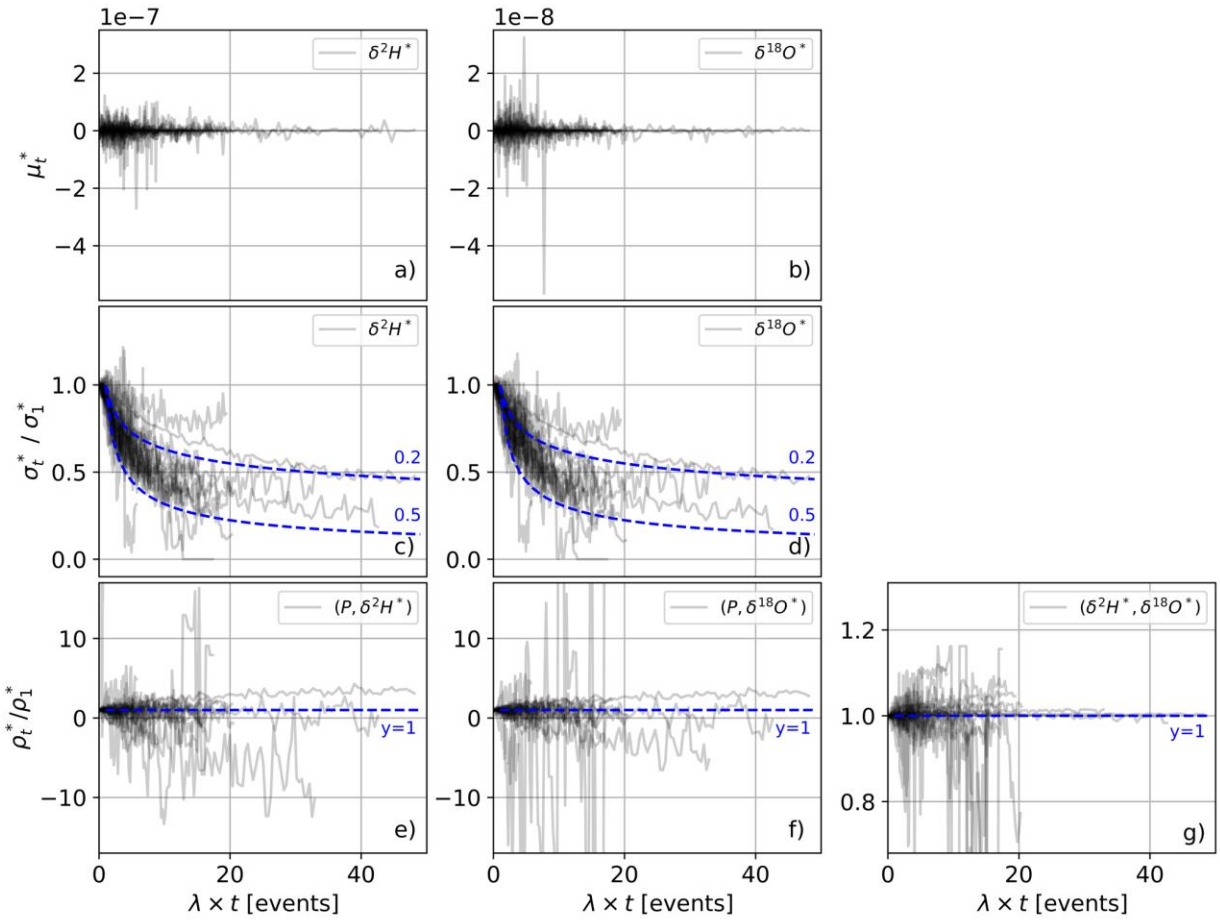

Figure 2. The x-axis is $\boldsymbol{\lambda}$ (recorded events / number of days in the time series) multiplied by daily to 12-week aggregation intervals (days) and the y-axes were the deviations for each of the 27 sites in their stochastic time series a,b) means ($\boldsymbol{\mu_t^*}$; note the scale of the y-axis), c,d) standard deviations at *t*-day ($\boldsymbol{\sigma_t^*}$) divided by the daily standard deviation ($\boldsymbol{\sigma_1^*}$) with blue dashed lines at $(\boldsymbol{\lambda n})^{\mathbf{0.5}}$ and $(\boldsymbol{\lambda n})^{\mathbf{0.2}}$, and e-g) Pearson correlation coefficients at *t*-day divided by daily ($\boldsymbol{\rho_t^*/\rho_1^*}$) with blue dashed lines at y-axis = 1. Refer to *Supplemental Materials* (Fig. S1) for larger ranges in y-axis values for ($\boldsymbol{\rho_t^*/\rho_1^*}$).

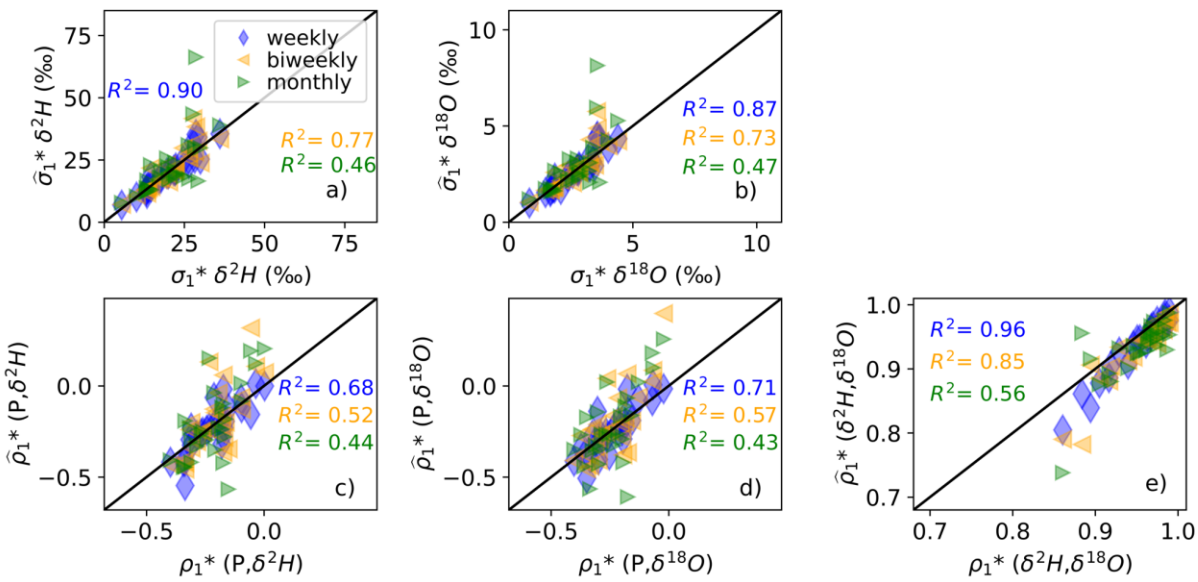

898

899 Figure 3. The estimated standard deviations (a,b) and Pearson correlation coefficients (c-e) of
900 the stochastic signal from downscaled weekly, biweekly and monthly time series compared to
901 the observed daily stochastic statistics. Each data point is one site location and the black lines are
902 the 1:1 lines. The means were not shown because they are approximately zero (refer to Figure
903 S2.a,b).

904

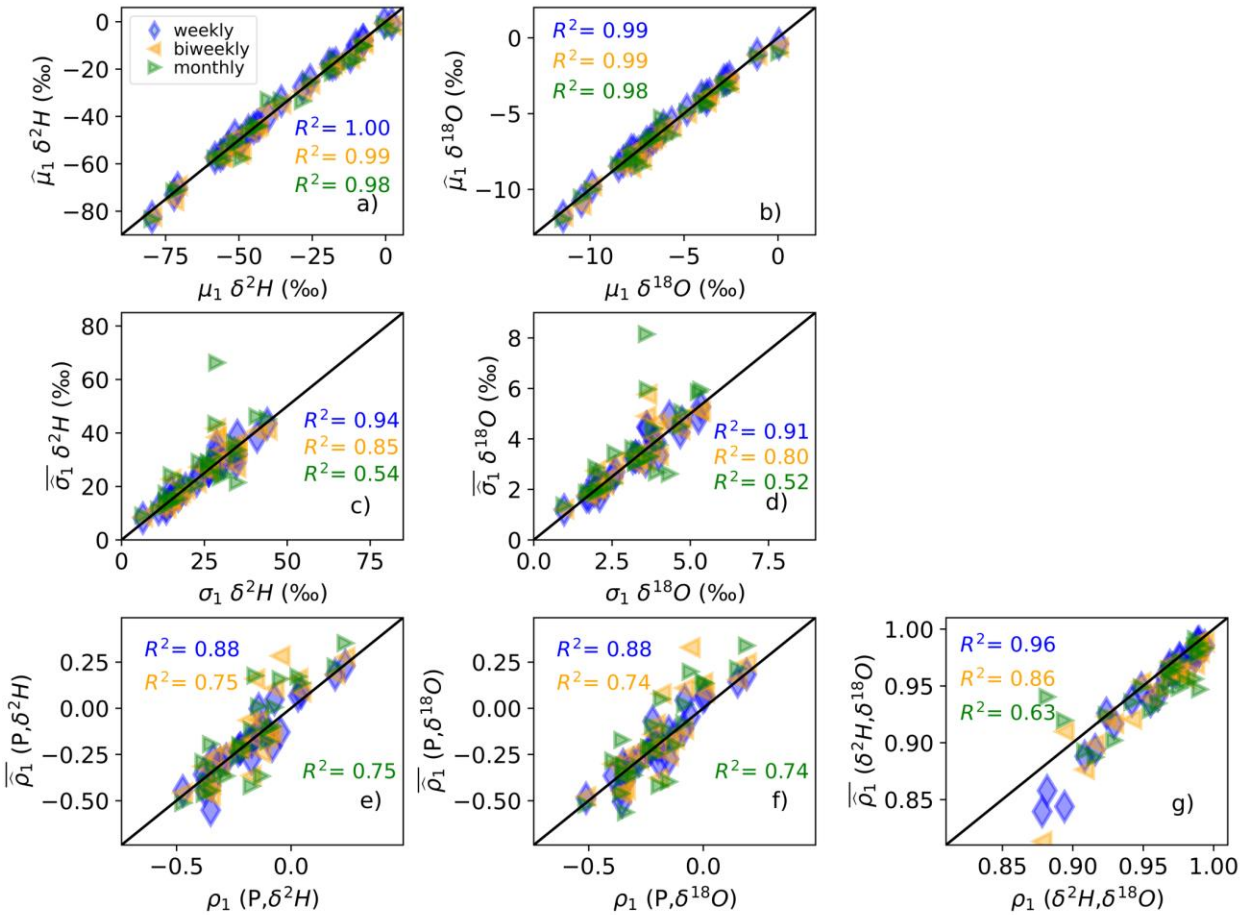

905

906 Figure 4. The average means (a,b), standard deviations (c,d) and Pearson correlation coefficients
907 (e-g) of the downscaled ensembles from the weekly, biweekly and monthly time series compared
908 to the observed daily site statistics. Each data point is one location and the black lines are the 1:1
909 lines.

910

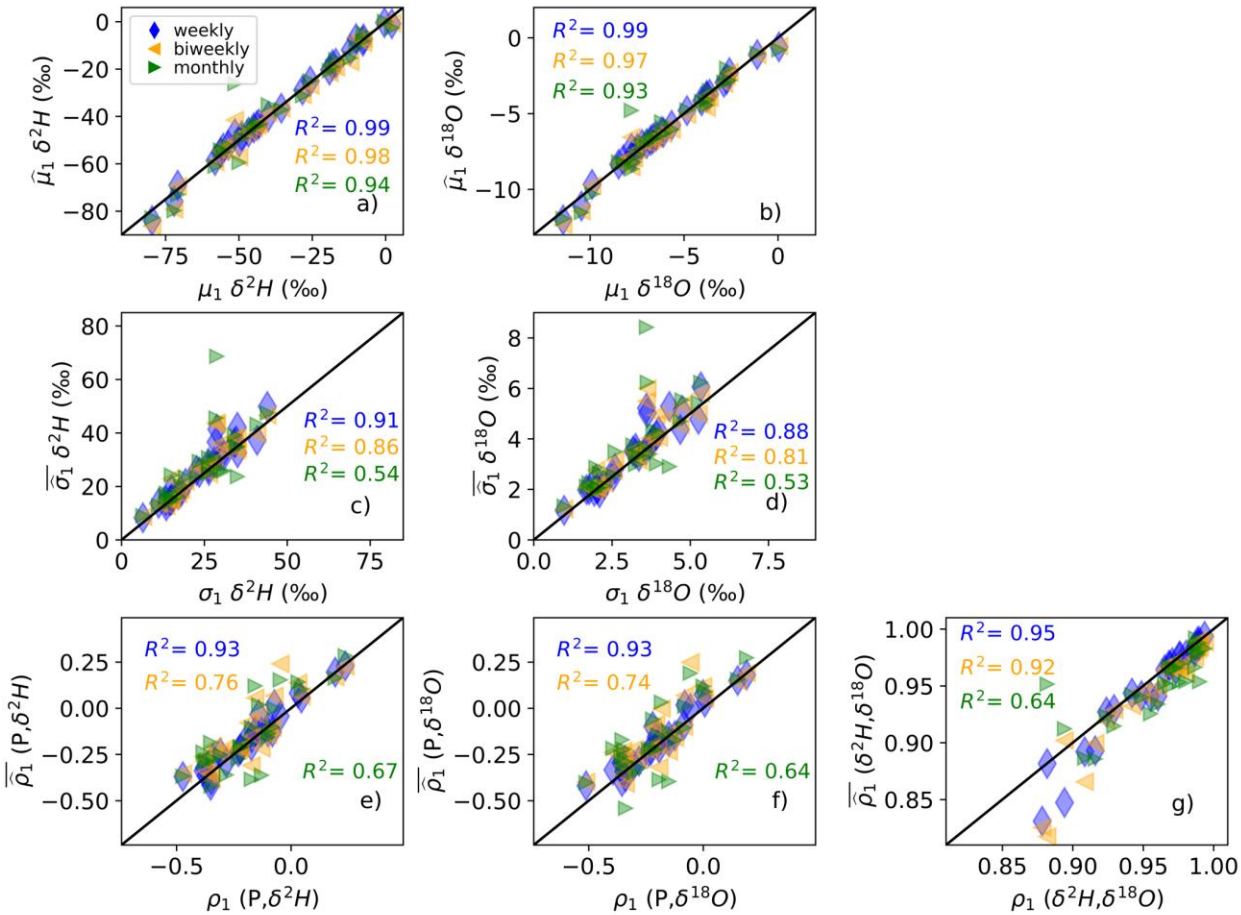

911

912 Figure 5. The average means (a,b), standard deviations (c,d) and Pearson correlation coefficients
913 (e-g) of the residual corrected downscaled ensembles from the weekly, biweekly and monthly
914 time series compared to the observed daily site statistics. Each data point is one location and the
915 black lines are the 1:1 lines.

916

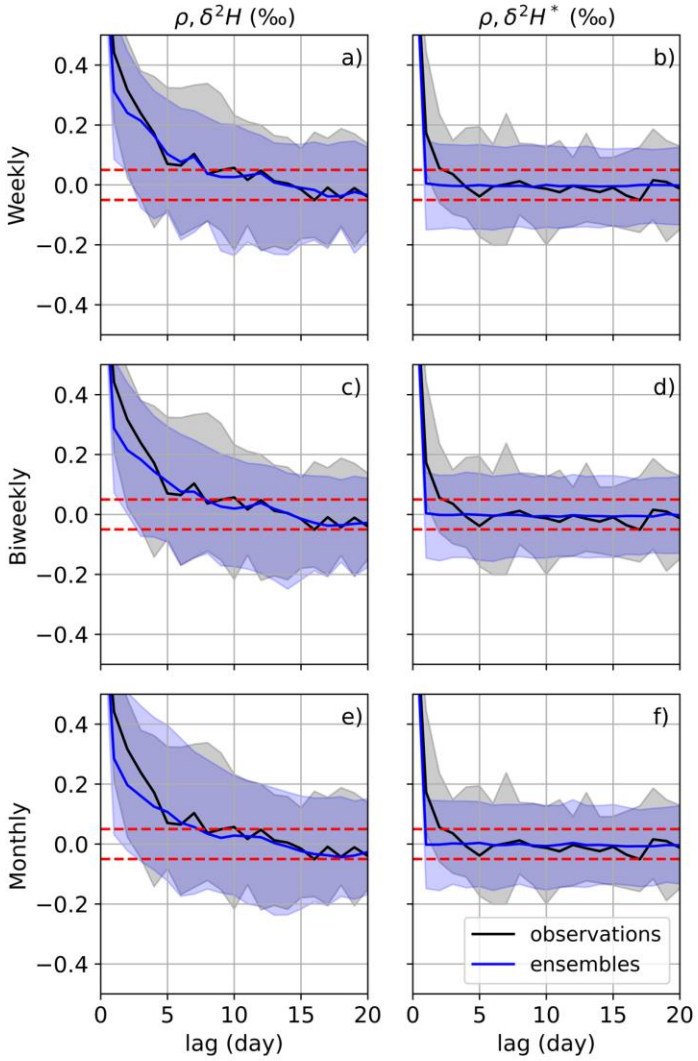

Figure 6. a,c,e) Median autocorrelation of the observed daily $\boldsymbol{\delta^2 H}$ datasets and the daily residual corrected ensembles (solid lines). b,d,f) Median autocorrelations of the $\boldsymbol{\delta^2 H^*}$ stochastic signals for the observations and the downscaled ensembles. The 5th to 95th percentiles of the observed and ensemble autocorrelations are represented as shaded regions. Horizontal red dashed line indicates where $\boldsymbol{\rho}$ is +/-5%.

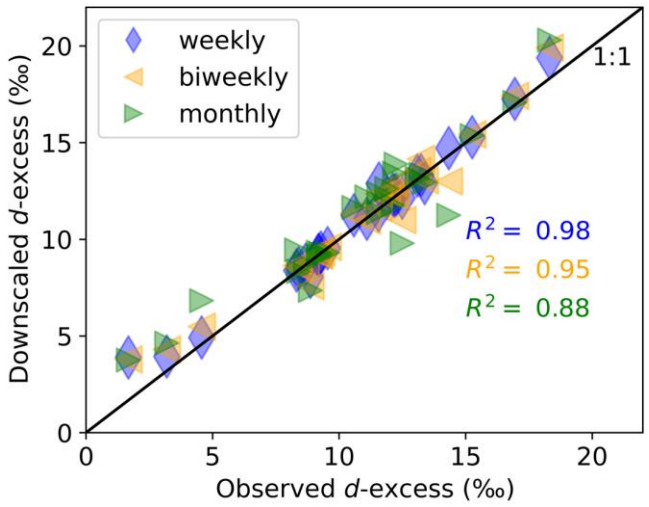

924

925 Figure 7. The average *d*-excess of the residual corrected downscaled ensemble at each site location

926 compared to the average observed *d*-excess. Each data point is one site location and the black line

927 is the 1:1 line.

928

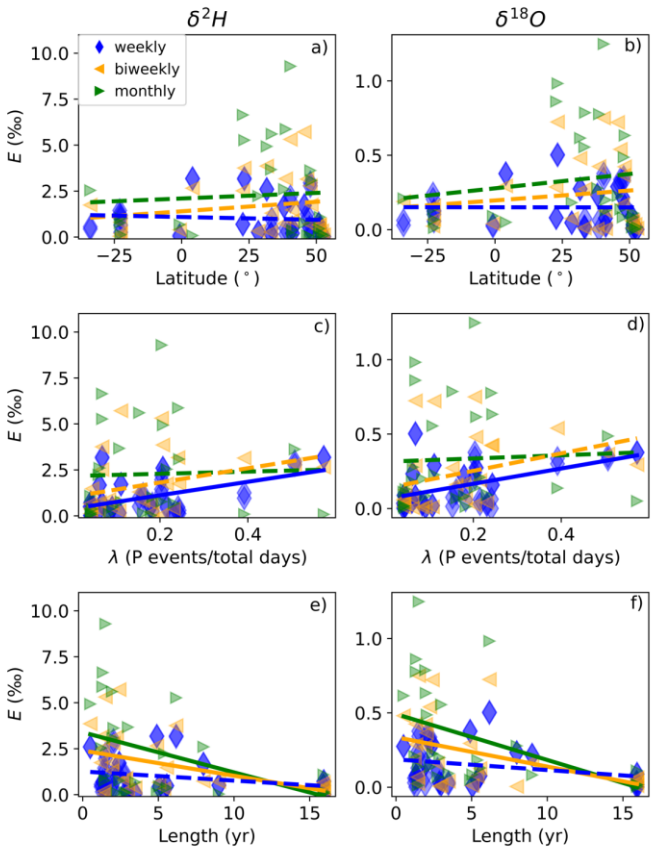

929

930 Figure 8. Absolute error (E) of the residual corrected ensemble means compared to various site-
931 specific characteristics: a,b) latitude, c,d) $\boldsymbol{\lambda}$, and e,f) total length of the time series. Each data
932 point is one site location, dashed lines represent p-values > 0.05, and solid lines represent p-
933 values < 0.05.

934

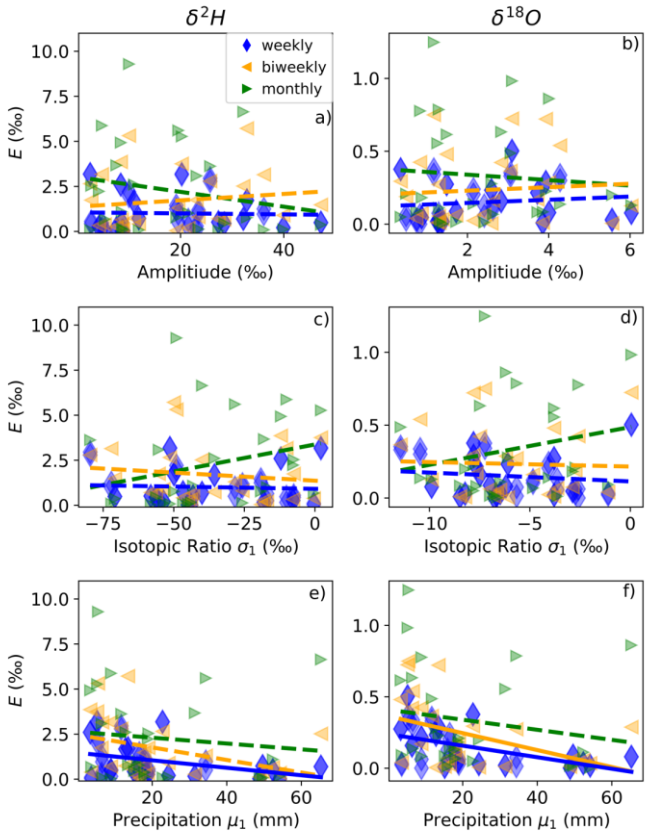

935

936 Figure 9. Absolute error (E) of the residual corrected ensemble means compared to various site-
937 specific characteristics: a,b) the sinusoidal function's estimated amplitude, c,d) standard deviation
938 of each isotope ratio and e,f) average daily precipitation. Each data point is one site location,
939 dashed lines represent p-values > 0.05, and solid lines represent p-values < 0.05.